Nanoscale

Multifunctional Molecular Charge-Transfer Thin Films

Journal:	*Nanoscale*
Manuscript ID	NR-ART-10-2019-008637
Article Type:	Paper
Date Submitted by the Author:	08-Oct-2019
Complete List of Authors:	Xu, Beibei; University at Buffalo - The State University of New York Li, Zheng; University at Buffalo - The State University of New York Chang, Shuquan; Nanjing University of Aeronautics and Astronautics, College of Materials Science and Technology; Nanjing University of Aeronautics and Astronautics, Jiangsu Engineering Laboratory of Nuclear Energy Equipment Materials Ren, Shenqiang; University at Buffalo - The State University of New York,

ARTICLE

Multifunctional Molecular Charge-Transfer Thin Films

Beibei Xu,[a,b] Zheng Li,[a,b,c] Shuquan Chang,[c] and Shenqiang Ren [a,b,d]*

Received 00th January 20xx,
Accepted 00th January 20xx

DOI: 10.1039/x0xx00000x

We report the controlled interfacial interaction in the crystallized organic charge tranfer thin films, consisting of bis(ethylenedithio)tetrathiafulvalene and C_{60}. The induced broad-band absorption from UV to near-infrared enables the wavelength dependent ambipolar (negative/positive) photoresponse, while multi-stimuli responsive behavior is achieved through the charge-transfer interactions. In addition, by coupling with tetrathiafulvalene-(7,7,8,8-tetracyanoquinodimethane) charge transfer complex, it shows a significantly increased conductivity. The controlled interfacial changer transfer interaction provides an efficient approach to obtain multifunctional molecular crystallized thin films with superior external stimuli response.

The supramolecular assembly of electron donor and acceptor into charge transfer (CT) crystals by noncovalent interaction affords great opportunities to achieve long-range ordered packing structure for unique physicochemical properties.[1-5] The modulation of stacking arrangement and CT degree between electron donor and acceptor provides an efficient approach to engineer interfacial coupling for the control of magnetic and electric order parameters in various applications, including thermoelectric, magnetoelectric, ferroelectric, light emitting diode, transistor, photoconductor, and so on.[2-4, 6-10] However, the strong intermolecular CT interaction often leads the self-assembly into molecular rigid single crystals which limit the thin film important device applications.[11] A variety of approaches have been proposed for the fabrication of molecular crystallized thin films, including multiple well-developed solution coating technology,[12-15] inkjet printing technology,[16] and so on. However, the complex processes are prohibitive for large-scale applications, such as the application of halogenated solvents, the rheological and flowability demands of printable ink, etc. A universal strategy is required for scalable fabrication of highly ordered molecular crystallized thin films. Moreover, the in-depth investigation of the interfacial CT interaction and molecular ordering between electron donor and acceptor and the effects on the electronic properties are vital importance.[17] Here, we develop a sublimation approach by evaporating molecular CT single crystal formed from bis(ethylenedithio)tetrathiafulvalene (BEDT-TTF) donor and C_{60} acceptor to deposit the crystallized thin films for the controlled interfacial CT interaction with multi-stimuli response. Compared with the methods of thermal evaporation of individual source, our approach uses one heating boat without the need to control evaporation parameters of each source. Moreover, by coupling with the metallic tetrathiafulvalene (TTF)-7,7,8,8-tetracyanoquinodimethane (TCNQ) cocrystal phase,[18] we demonstrate the enhanced conductivity resulted from the coupling effect between (BEDT-TTF)C_{60} (BCCT) and TTF-TCNQ (TQ).

Figure 1a and the inset show scanning electron microscopy (SEM) and optical microscopy (OM) images of BCCT single crystal prepared by chemical bath deposition method, which exhibits several hundred micrometers wide and millimeters long. Figure 1b displays the sublimation setup for the preparation of BCCT thin film, in which the BCCT thin films can be deposited on various substrates (Fig. 1b-1e and S1-S10). With the increase of the sublimation temperature, we observe the increased density and dimension of phase separated structure, while the BCCT thin film becomes thicker. Energy dispersive X-ray spectroscopy (EDS) indicates that the island area is rich in carbon and sulfide elements (the inset of Fig. 1e). The comparison of EDS element mapping indicates that the increase of deposition temperature leads to a higher density of phase separated structure rich in the sulfide element (the inset of Fig. 1d, S8 and S10). As shown in Fig. 1f and 1g, BEDT-TTF crystal is of monoclinic structure, while C_{60} crystal is of cubic structure, raising the possibility of forming phase separated BCCT structure. The temperature dependent phase separation is evaluated and shown in Fig. 1h, in which the phase separation and the ratio of BEDT-TTF phase increases with the increase of the deposition temperature from 235 to 400 ^{o}C. The ratio of BEDT-TTF to C_{60} reaches 1:1 at 300 ^{o}C. At a low temperature (the step 1 in Fig. 1i), the

[a] *Department of Mechanical and Aerospace Engineering, University at Buffalo, The State University of New York, Buffalo, NY, 14260, USA*
[b] *Research and Education in energy, Environment and Water (RENEW) Institute, University at Buffalo, The State University of New York, Buffalo, NY, 14260, USA*
[c] *College of Material Science and Technology, Nanjing University of Aeronautics and Astronautics, Nanjing, 210016, China.*
[d] *Department of Chemistry, University at Buffalo, The State University of New York, Buffalo, NY, 14260, USA*
E-mail: Shenqiang Ren(shenren@buffalo.edu)
Electronic Supplementary Information (ESI) available: [Optical microscopy images, Scanning electron microscopy images, I-V curves and photocurrent response]. See DOI: 10.1039/x0xx00000x

deposited film contains larger amount of BEDT-TTF than that of C_{60}, leading to non-equivalent phase separation with weak interfacial interaction. The increased temperature leads to the large amount of C_{60} with more homogenously distributed BEDT-TTF and C_{60} across the thin film, causing an increased interfacial coupling (the step 2 in Fig. 1i). However, further increasing the temperature results in the aggregation and phase segregation as shown for thin film deposited at 400 °C (Fig. 1e), resulting in a weak interfacial interaction (the step 3 in Fig. 1i).

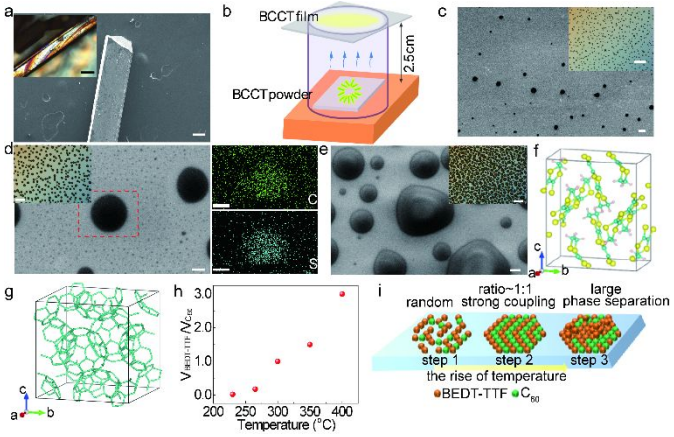

Figure 1 Morphology of the crystallized (BEDT-TTF)C_{60} (BCCT) charge transfer (CT) thin film. a, Scanning electron microscopy (SEM) image of BCCT crystals. The inset is the optical microscopy (OM) image. b, The sublimation setup for the fabrication of molecularly crystallized BCCT thin film. c-e, SEM images of the film at a sublimation temperature of 230, 300 and 400 °C for 1.5 h, respectively. The inset is the enlarged OM images. The right insets in Fig. 1d are the energy dispersive X-ray spectroscopy element mapping for carbon and sulfide elements. The scale bars in Figs. 1a, 1c-1e, are 100, 2, 1 and 1 μm, respectively. The scale bar in the insets of Figs. 1a, 1c-1e are 200, 10, 10 and 10μm, respectively. f-g, Crystal packing structure of BEDT-TTF and C_{60}, respectively. h, Sublimation temperature dependent phase separation extent. i, Temperature dependent growth and phase separation process of crystallized BCCT film.

The BCCT thin film demonstrates the diode behavior with the optimum conductivity of 3.26×10^{-9} S cm^{-1} under 50% phase separation (Fig. 2a). Due to the quantum confinement effect and the large surface-to-volume ratio,[19] the crystallized BCCT thin film displays broad absorption covering from UV to near-infrared region with two pronounced absorption peak at 310 and 440 nm (Fig. 2b). The broad absorption endows BCCT thin film with broadband photoresponse from UV to near-infrared region (Fig. 2c), where BCCT thin film demonstrates the wavelength dependent ambipolar (positive/negative) photoresponse. Figure 2d shows the photocurrent change with light on and off for both 365 and 850 nm. It shows light wavelength dependent ambipolar photoresponse behaviour which should be related to impurity levels. The positive photoresponse in such wavelength dependent ambipolar photoresponse is related to the photogenerated charge carriers,[20, 21] while the negative photoresponse may be related to the trapping of photogenerated electrons by impurity level above the mobility edge and the defect states in the forbidden band where recombination of the photogenerated electrons with the localized acceptor impurity energy level in the forbidden band leads to the decrease of conductivity below the dark level.[20] On the other hand, a transient increase or decrease of electrical current behaviour occurs with the light on and off (Fig. 2d), which can be explained by the modified Stöckman model where the localized acceptor energy level in the forbidden band plays an important role.[20, 22] With the light illumination, photogenerated holes give rise to the positive photocurrent before being trapped by the localized acceptor energy level in the forbidden band. Holes cannot be created after the light is off, leading to the decrease of the current density. Similar to the positive photoresponse, light intensity dependent negative photoresponse also shows linear behaviour, indicating the trapping of photocarriers (Fig. 2e).[23] As shown in Fig. 2f, the phase separation has large influence on the photoresponsibility, revealing the interfacial coupling interaction between BEDT-TTF and C_{60}. In consistent with the above discussion, the film with the strong interfacial interaction shows the optimum photoresponsibility. Thus, by controlling the phase separation, the polarity of photoresponse can be controlled (Fig. S13).

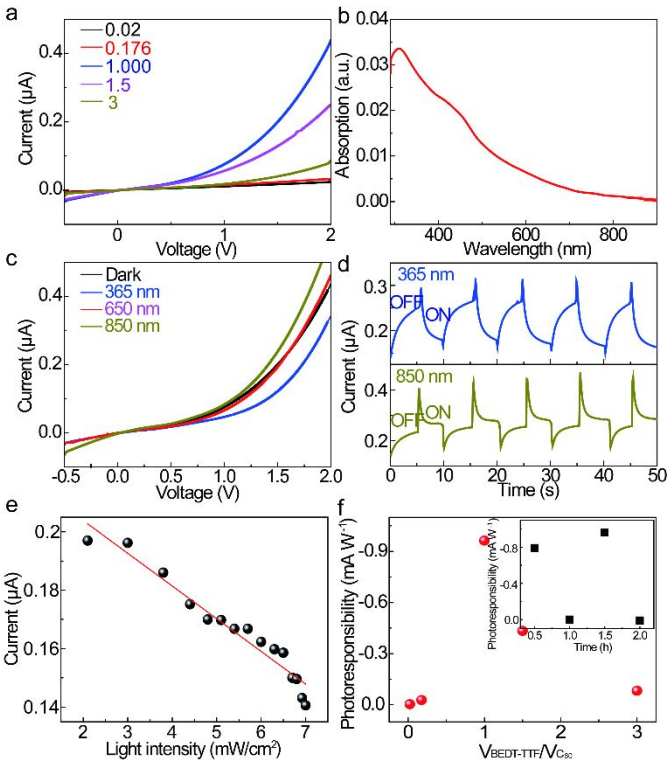

Figure 2 Optical and photoresponse properties of BCCT crystallized film. a, Current-voltage curves of the films sublimated for different deposition time. b, Absorption spectra of the film sublimated at 300 °C for 1.5 h. c, Current-voltage curves of the films sublimated at 300 °C for 1.5 h under dark and different light illumination. The light intensity is 6.5 mW/cm^2. d, Photocurrent response with light on and off for the light wavelength of 650 and 850 nm. e, Light intensity dependent photocurrent under 365 nm. f, Photoresponsibility of the film with different phase seperation and the film sublimated at 300 °C for different time.

The small dielectric constant of BCCT facilitates the formation of relatively large Coulomb capture radius $r=e^2/(4\pi\varepsilon_0\varepsilon_r\kappa_B T)$, where e is the electron charge, ε_0 is the vacuum dielectric constant, ε_r is the relative dielectric constant, κ_B is the Boltzman constant, T is the temperature.[10, 24, 25] Thus, electrons and holes can be captured with the formation of the CT states. Moreover, a strong interfacial interaction is beneficial for the formation of CT states. There are energy difference between singlet and triplet CT states, and the application of magnetic field induces Zeeman splitting effect to decrease the energy difference between singlet and triplet CT states to control their intersystem crossing for the tuning of charge carriers, enabling external stimuli dependent response in this material system.[26] To explore magnetic field effects, magnetoconductance (MC) under dark and light is compared (Fig. 3a). The MC value is negative under dark and positive under light illumination, and it increases with the increase of magnetic field and light intensity (Fig. 3b). Under the magnetic field, the intersystem crossing from singlet to triplet CT leads to the density increase of triplet excitons and polarons. The increased scattering interaction with the decrease of the mobility of polarons lead to the decrease of electrical current. By contrast, under photoexcitation, the excitons can be dissociated into free charge carriers by the interaction with polarons, resulting in the enhanced current density. With the increase of light intensity, the dissociation of excitons by polarons can be increased, leading to the increase of MC. As the lifetime of triplet excitons (>μs) is much longer than that of singlet excitons (ps~ns),[27, 28] the triplet excitons mainly contributes to the formation of dipoles, naming the capacitance of BCCT thin films. Thus, the increased density of triplet CT can partially transfer to triplet excitons under photoexcitation with the increase of the capacitance (Fig. 3c). In addition, the tuning of the density of triplet excitons by external magnetic field can inevitably cause the change of the capacitance (Fig. 3c and 3d).

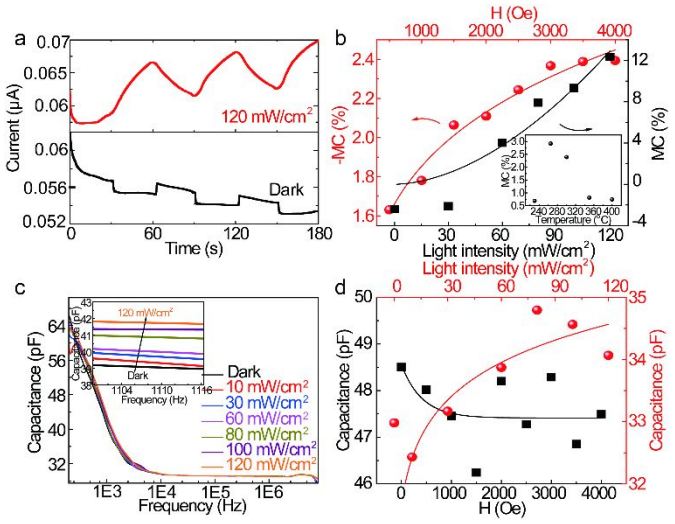

Figure 3 Magnetic field and light sensing ability of the crystallized film. a, The tuning of current with magnetic field on and off under dark and a light intensity of 120 mW/cm². b, Magnetic field and light intensity dependent magnetoconductance (MC) change. The inset is MC for the film sublimated at different temperatures. c, Frequency dependent capacitance change under dark and different light illumination. d, Magnetic field and light intensity dependent capacitance change at 700 Hz.

Till now, much effort has been devoted to enhance the carrier mobility of molecular CT solids, such as the control of molecular packing and chemical doping.[29, 30] Distinct from traditional approach, the coupling between metallic CT crystal TQ (Fig. 4a) and BCCT single crystal are examined. The BCCT film is deposited on the top of TQ crystallized thin film (Fig. 4b and the inset). The conductivity is much higher than that of BCCT crystallized thin film (Fig. S23). Conducting atomic force microscopy (c-AFM) images indicate the higher conductivity of the complex BCCT-TQ film (Fig. 4d) than that of BCCT film (Fig. 4c). The current-voltage curves obtained by the c-AFM probe tips (Fig. 4e) and normal device (Fig. S23) both confirm the higher conductivity of the complex BCCT-TQ film. Figures 4f illustrates the conductivity mechanism of molecular BCCT-TQ complex film. By contrast, the needle-like highly conductive TQ crystals form three-dimensional network of high continuity within the BCCT thin film matrix, resulting in high conductivity of the complex film. Besides, the complex film displays similar negative photoresponse to that of BCCT film under solar light (Fig. S24).

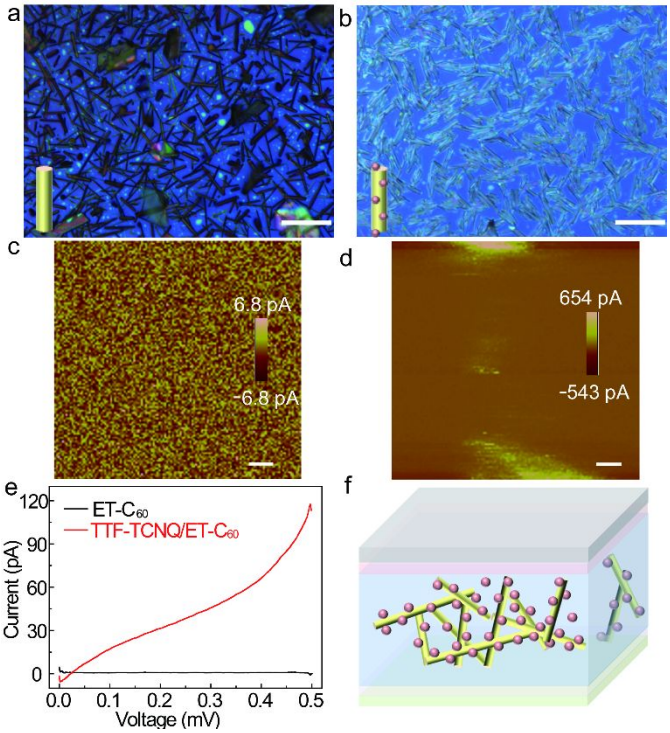

Figure 4 The coupling behaviour with enhanced conductivity of TTF-TCNQ (TQ) and BCCT crystallized film. a-b, OM images for TQ crystallized film and TQ/BCCT complex film, respectively. c-d, Conducting atomic force microscopy (c-AFM) images for BCCT crystallized film and TQ/BCCT complex film, respectively. e, Current-voltage curves of BCCT crystallized film and TQ/BCCT complex film obtained from c-AFM. f, Schematic illustration of the distribution and conduction mechanism for TQ/BCCT complex film.

Conclusions

In conclusion, the crystallized (BEDT-TTF)C_{60} thin film shows broad absorption and photoresponse from UV to near-infrared region, while the interaction of photogenerated carriers with the localized defect acceptor level induces the light wavelength dependent ambipolar (negative/positive) photoresponse. Moreover, we observe the charge transfer characteristic with magnetic field effect and photoexcitation dependent conductance and capacitance. Moreover, the coupling between TTF-TCNQ and (BEDT-TTF)C_{60} endows the complex thin film with high conductivity than that of (BEDT-TTF)C_{60} crystallized film. The interfacial interaction and the coupling between organic charge transfer crystals is promising to be applied for multifunctional molecular films with improved optoelectronic properties.

Experimental Section

The preparation of (BEDT-TTF)C_{60} and TTF-TCNQ charge transfer crystallized film: (BEDT-TTF)C_{60} crystals were prepared by chemical bath deposition method.[10] 7 mg/mL BEDT-TTF (Tokyo Chemical Industry Co., LTD) and C_{60} (Sigma-Aldrich Co.) were dissolved in 1,2-dichlorobenzene solvent and kept stable at 80°C for 5 h. After that, needle-like black (BEDT-TTF)C_{60} single crystal formed at the bottom of the solution. The crystals were dried under N_2 at 80°C. 5 mg/mL TTF (Tokyo Chemical Industry Co., LTD) and TCNQ (Sigma-Aldrich Co.) was dissolved in acetonitrile (ACN) solvent and stirred for 3h till the percipitation of small black needle-like crystals and dried under N_2 at 80 °C. For the sublimation of crystallized film, TTF-TCNQ crystals were heated at 230 °C for 1.5 h, (BEDT-TTF)C_{60} crystals were heated at different temperatures from 230 to 400 °C for 0.5~2 h.

Electrical and dielectric properties characterization:Current and voltage signals was obtained by CHI 422 Series Electrochemical Workstation. Agilent 4294a Precision impedance equipment with 16047E fixture was used to caputure frequency dependent capacitance from 40 Hz to 10 MHz at 0.2 V.

Conducting atomic force microscopy (c-AFM) measurement: Current mapping was taken on the crystals by Bruker dimension icon under contacting mode with Si probe coated by Pt/Cr electrode. The scanning rate is 1μm/s.

Conflicts of interest

The authors declare no competing financial interests.

Acknowledgements

The U.S. Department of Energy, Office of Basic Energy Sciences, Division of Materials Sciences and Engineering supports S.R. under Award DE-SC0018631 (Organic conductors). Financial support was provided by the U.S. Army Research Office supports S. R. under Award W911NF-18-2-0202 (Materials-by-Design and Molecular Assembly).

References

1. A. K. Blackburn, A. C. H. Sue, A. K. Shveyd, D. Cao, A. Tayi, A. Narayanan, B. S. Rolczynski, J. M. Szarko, O. A. Bozdemir, R. Wakabayashi, J. A. Lehrman, B. Kahr, L. X. Chen, M. S. Nassar, S. I. Stupp and J. F. Stoddart, Journal of the American Chemical Society, 2014, 136, 17224-17235.
2. W. Zhu, R. Zheng, X. Fu, H. Fu, Q. Shi, Y. Zhen, H. Dong and W. Hu, Angewandte Chemie International Edition, 2015, 54, 6785-6789.
3. A. S. Tayi, A. K. Shveyd, A. C. H. Sue, J. M. Szarko, B. S. Rolczynski, D. Cao, T. J. Kennedy, A. A. Sarjeant, C. L. Stern, W. F. Paxton, W. Wu, S. K. Dey, A. C. Fahrenbach, J. R. Guest, H. Mohseni, L. X. Chen, K. L. Wang, J. F. Stoddart and S. I. Stupp, Nature, 2012, 488, 485-489.
4. J. Zhang, H. Geng, T. S. Virk, Y. Zhao, J. Tan, C.-a. Di, W. Xu, K. Singh, W. Hu, Z. Shuai, Y. Liu and D. Zhu, Advanced Materials, 2012, 24, 2603-2607.
5. T. Enoki and A. Miyazaki, Chemical Reviews, 2004, 104, 5449-5478.
6. K. Harada, M. Sumino, C. Adachi, S. Tanaka and K. Miyazaki, Applied Physics Letters, 2010, 96, 253304.
7. B. Xu, H. Li, H. Li, A. J. Wilson, L. Zhang, K. Chen, K. A. Willets, F. Ren, J. C. Grossman and S. Ren, Nano Letters, 2016, 16, 2851-2859.
8. H. Alves, R. M. Pinto and E. S. Maçôas, Nat Commun, 2013, 4, 1842.
9. S. J. Kang, S. Ahn, J. B. Kim, C. Schenck, A. M. Hiszpanski, S. Oh, T. Schiros, Y.-L. Loo and C. Nuckolls, Journal of the American Chemical Society, 2013, 135, 2207-2212.
10. B. Xu, Z. Luo, W. Gao, A. J. Wilson, C. He, X. Chen, G. Yuan, H.-L. Dai, Y. Rao, K. Willets, Z. Dauter and S. Ren, Chemistry of Materials, 2016, 28, 2441-2448.
11. Y. L. Lei, L. S. Liao and S. T. Lee, Journal of the American Chemical Society, 2013, 135, 3744-3747.
12. Y. Diao, B. C. K. Tee, G. Giri, J. Xu, D. H. Kim, H. A. Becerril, R. M. Stoltenberg, T. H. Lee, G. Xue, S. C. B. Mannsfeld and Z. Bao, Nat Mater, 2013, 12, 665-671.
13. C. W. Sele, B. K. C. Kjellander, B. Niesen, M. J. Thornton, J. B. P. H. van der Putten, K. Myny, H. J. Wondergem, A. Moser, R. Resel, A. J. J. M. van Breemen, N. van Aerle, P. Heremans, J. E. Anthony and G. H. Gelinck, Advanced Materials, 2009, 21, 4926-4931.
14. H. A. Becerril, M. E. Roberts, Z. Liu, J. Locklin and Z. Bao, Advanced Materials, 2008, 20, 2588-2594.
15. H. Li, B. C. K. Tee, G. Giri, J. W. Chung, S. Y. Lee and Z. Bao, Advanced Materials, 2012, 24, 2588-2591.
16. H. Minemawari, T. Yamada, H. Matsui, J. y. Tsutsumi, S. Haas, R. Chiba, R. Kumai and T. Hasegawa, Nature, 2011, 475, 364-367.
17. T. He, X. Zhang, J. Jia, Y. Li and X. Tao, Advanced Materials, 2012, 24, 2171-2175.
18. J. Ferraris, D. O. Cowan, V. Walatka and J. H. Perlstein, Journal of the American Chemical Society, 1973, 95, 948-949.
19. R. B. Jacobs-Gedrim, M. Shanmugam, N. Jain, C. A. Durcan, M. T. Murphy, T. M. Murray, R. J. Matyi, R. L. Moore and B. Yu, ACS Nano, 2014, 8, 514-521.
20. W. Liu, J.-S. Lee and D. V. Talapin, Journal of the American Chemical Society, 2013, 135, 1349-1357.
21. J. Yoo, J. Pyo and J. H. Je, Nanoscale, 2014, 6, 3557-3560.
22. F. Stöckmann, Zeitschrift für Physik, 1955, 143, 348-356.
23. H. Kind, H. Yan, B. Messer, M. Law and P. Yang, Advanced Materials, 2002, 14, 158-160.
24. L. Onsager, Physical Review, 1938, 54, 554-557.
25. T. M. Clarke and J. R. Durrant, Chemical Reviews, 2010, 110, 6736-6767.
26. B. Hu, L. Yan and M. Shao, Advanced Materials, 2009, 21, 1500.

27. C. Silva, Nat Mater, 2010, 9, 884-885.
28. M. A. Baldo, D. F. O'Brien, Y. You, A. Shoustikov, S. Sibley, M. E. Thompson and S. R. Forrest, Nature, 1998, 395, 151-154.
29. G. Giri, E. Verploegen, S. C. B. Mannsfeld, S. Atahan-Evrenk, D. H. Kim, S. Y. Lee, H. A. Becerril, A. Aspuru-Guzik, M. F. Toney and Z. Bao, Nature, 2011, 480, 504-508.
30. G. Lu, J. Blakesley, S. Himmelberger, P. Pingel, J. Frisch, I. Lieberwirth, I. Salzmann, M. Oehzelt, R. Di Pietro, A. Salleo, N. Koch and D. Neher, Nat Commun, 2013, 4, 1588.